Strain distribution and optical phonons in InAs/InP self-assembled quantum dots

J. Groenen
Laboratoire de Physique des Solides, ESA 5477, Université P. Sabatier, F-31062 Toulouse Cedex 4, France

C. Priester
IEMN, Département ISEN, CNRS-UMR 8520, BP 69 F-59652 Villeneuve d'Ascq Cedex, France

R. Carles
Laboratoire de Physique des Solides, ESA 5477, Université P. Sabatier, F-31062 Toulouse Cedex 4, France
(Received 14 June 1999)

The strain distribution in self-assembled InAs/InP (001) quantum dots is calculated, using an atomistic valence force-field description. Two typical dot shapes are considered. Strain relaxation is found to depend much on the dot shape. From these modeling results we deduce the strain-induced phonon frequency shifts. Unlike confinement, strain induces large frequency shifts. The calculations agree well with experimental results obtained by Raman scattering. It is shown that alloying effects are small. Finally, we show that average strain values can be obtained experimentally if one combines longitudinal and transverse optical-phonon Raman scattering. [S0163-1829(99)10347-3]

I. INTRODUCTION

Self-assembled quantum dot structures have been attracting considerable attention in the past decade. Dots are obtained during heteroepitaxy as a result from the elastic relaxation of misfit strain. Several studies were devoted to the modeling of the strain inside the dots.[1–6] Calculations were performed using either elastic continuum theory (finite element model)[1–3] or an atomistic description [valence force field model (VFF)].[4–6] The strain field was shown to depend strongly on dot shape. Thanks to the strain simulations, the quantitative analysis of many experimental data has become possible. In particular, they are very helpful to understand the electronic properties.[2,3,5,6] Confinement effects were shown (see, for instance, Ref. 6) to depend strongly on dot size and strain (and thus on the dot shape).

Although phonons are efficient probes for investigating low-dimensional structures, to date little work has been done on phonons in self-assembled nanostructures.[2,7–16] Most of the theoretical and experimental work on phonons in quantum dots deals with unstrained systems. Only a few Raman scattering investigations of self-assembled nanostructures have been reported.[9–16] Valuable information (about strain, alloying, electronic properties, . . .) has been accessed using resonant Raman scattering. In particular, Raman scattering was shown to provide a means of determining independently the residual strain and the alloy composition in SiGe/Si self-assembled dots.[13]

In this paper we shall address two issues. (i) How is the strain distributed in InAs/InP (001) self-assembled dots? (ii) How does it modify the optical-phonon frequencies? To answer the first question, we use the VFF model.[17] A large simulation cell is considered, in order to account for both the strain distribution inside and around the dots. In contrast with previous simulations of strain in capped dots, we shall examine capped dots with truncated pyramidal shapes. The strain-induced optical-phonon frequency shifts will be derived from the calculated strain. We shall finally compare these calculations to experimental results obtained by means of resonant Raman scattering on InAs/InP (001) self-assembled dots. In contrast with InAs/GaAs or $InP/In_xGa_{1-x}P$ systems, the gap between the InAs and InP optical-phonon frequencies is large. Consequently, the confinement of the InAs optical phonons inside the dots is very efficient, providing us with local probes. Moreover, the dot-related features can therefore be easily identified in the Raman spectra.

II. CALCULATIONS

A. Strain distribution

It should be noted that the accuracy of the VFF model goes beyond classical elasticity theory as it decribes the elastic properties and the relaxation on the atomic scale.[18] The strain elastic energy δE depends on the geometric deformations of bonds that each atom makes with its four nearest neighbors. For each atom i of the zinc-blende structure, one can write

$$\delta E_i = \sum_{j=1}^{4} \frac{3}{8r_0^2}\alpha[\vec{r}_{ij}^{\,2} - r_0^2]^2 + \sum_{j=1}^{4}\sum_{k=j+1}^{4} \frac{3}{8r_0^2}\beta\left[\vec{r}_{ij}\cdot\vec{r}_{ik} + \frac{r_0^2}{3}\right]^2. \tag{1}$$

$\vec{r}_{ij}$ is the vector connecting the central atom i to one of its four nearest neighbors j; r_0 is the unstrained bond length; α and β are, respectively, bond-bending and bond-stretching elastic constants. They are related to the elastic constants c_{11}, c_{12}, and c_{44} of the continuum elasticity theory by the following expressions:

$$c_{11} = \frac{\alpha + 3\beta}{a}, \quad c_{12} = \frac{\alpha - \beta}{a}, \quad c_{44} = \frac{4\alpha\beta}{a(\alpha+\beta)}. \tag{2}$$

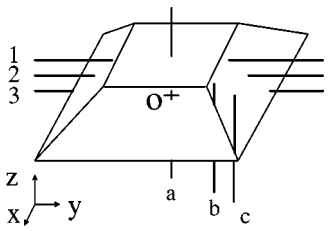

FIG. 1. Schematic plot of a type-*A* pyramid. The origin *O* is the center of the pyramid base plane. $x=[110]$, $y=[1\bar{1}0]$, and $z=[001]$.

$a=4r_0/\sqrt{3}$ is the lattice constant. It is not possible to perfectly fit all three c_{ij}'s with only two elastic constants α and β; the less ionic is the material, the better is the fit. Thus, this method basically works with covalent bonding, but Coulomb corrections could be introduced.[19] In practice, for the sake of simplicity one usually simply uses Eq. (1).[20] This we do, and choose to fit c_{11} and c_{12} and to drop c_{44}, resulting in a 10–20 % error range on the VFF effective c_{44}.

We examine two typical InAs/InP (001) dot morphologies, corresponding to the ones already reported in Refs. 10 and 21. The misfit strain between InAs and InP equals -3.1%. The first morphology, labeled *A*, corresponds to 3 nm high and 25 nm wide dots, whereas the second one, labeled *B*, corresponds to 7 nm high and 45 nm wide dots. The dots have truncated pyramidal shapes, with (114) and (113) side facets for *A* and *B*, respectively. InAs islands are formed on the top of a 1.5 monolayer (ML) wetting layer (WL) and capped by a 25 nm InP layer.[10,21]

For the sake of simplicity, we simulate pyramids with square base (the InAs/InP islands are in fact slightly elongated along $[1\bar{1}0]$ (Ref. 21)), and periodic boundary conditions in the plane perpendicular to [001] are used. At the bottom of the modelized cell, atoms are kept fixed, in order to simulate the thick substrate. We calculate the atomic positions that minimize the total elastic energy. Once the positions of all atoms are known, the local deformation distribution is derived straightforwardly. Calculations have been performed with and without WL (1 or 2 ML thick). Concerning the strain field in the dots, no significant differences were observed. The results we present here were obtained disregarding the WL. It has been shown that the subtrate and the cladding layer are affected by the strain relaxation within the dot. In particular, the strain field penetrates deeply into the subtrate.[4] Consequently, to obtain a reliable and realistic strain field, a rather thick nonfrozen substrate layer has to be considered in the simulation. For that purpose, calculations have been performed with up to 600 000 atoms and about 95% of the simulation cell corresponds to InP. A small scaling factor (1.6 for *A* and 5 for *B*) remains between the actual pyramid size and the one used in the simulation. One can avoid this scaling factor but, in counterpart, one has to reduce the substrate layer thickness. We have checked, on smaller systems, the validity of using such a scaling factor, which is bound to the fact that the strain field depends much on shape and not on size.

Typical local deformation distributions within the dots (along lines defined in Fig. 1) are shown in Figs. 2 and 3 for shape *A*. Except close to the pyramid boundaries, the strain field is rather uniform and does not vary very rapidly. The

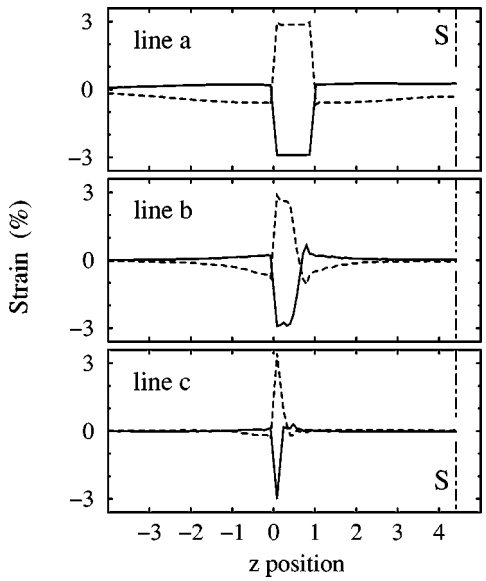

FIG. 2. Local deformations along the *a*, *b*, and *c* lines defined in Fig. 1: ε_{xx} (solid line) and ε_{zz} (dashed line). *z* positions are normalized with respect to the pyramid height ($z=0$ stands for the pyramid bottom and $z=1$ for the pyramid top). *S* denotes the sample surface.

shear strain ε_{ij} $(i\neq j)$ turns out to be significant at the facet edges and pyramid boundaries and very small inside the pyramid (Fig. 3). Let us point out that the previous simulations of strain in capped islands all correspond to untruncated pyramids. Unlike for capped untruncated pyramids, ε_{xx} and ε_{yy} never change sign inside the pyramid.[2,5]

Figure 2 clearly shows that the strain field penetrates deep into the InP barriers. At the surface of the InP capping layer, some strain is still present just above the dot (compare lines *a* and *b*). As this tensile strain is rather localized within the *xOy* plane, it is able to promote vertical order when several layers with dots are grown.[22]

From the numerical local deformation values of all the InAs cells, we have computed the average strain within the

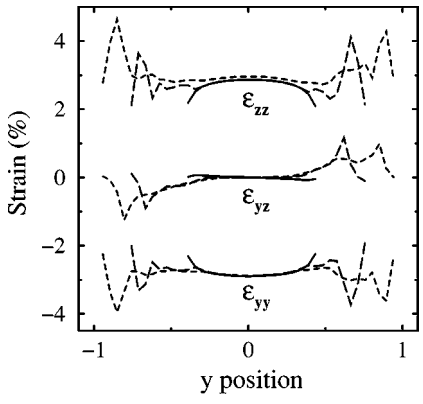

FIG. 3. Local deformations along the lines defined in Fig. 1: 1 (solid line), 2 (dashed line), and 3 (dotted line). *y* positions are normalized with respect to half of the pyramid base width ($y=0$ corresponds to the middle). ε_{xy} and ε_{xz} are not reported here as they equal almost zero regardless of the *y* position. ε_{xx} are not reported either; they display almost constant values, given by $\varepsilon_{xx}=\varepsilon_{yy}$ at $y=0$.

TABLE I. Average strain components for *A* and *B* dot shapes. 2D stands for a pseudomorphic InAs layer on InP.

Shape	ε_{xx}	ε_{yy}	ε_{zz}	$\varepsilon_{zz}/\varepsilon_{xx}$
2D	−3.1	−3.1	+3.4	−1.1
A	−2.81	−2.80	+2.67	−0.95
B	−2.62	−2.60	+2.18	−0.83

InAs dot. The average values of the diagonal strain components in the InAs dot are reported in Table I [the values corresponding to a pseudomorphic two-dimensional (2D) layer are also given as a reference]. According to symmetry requirements, the average values of the shear strain components vanish. The biaxial strain relationship, $\varepsilon_{zz}/\varepsilon_{xx} = -2C_{12}/C_{11}$, has often been assumed to be valid for flat islands. It is noteworthy that, even for the rather flat islands examined here, this relationship does not hold (Table I). Residual strain depends much on shape. The *B*-type dots are more relaxed than the *A*-type ones (their height/width ratio equals 0.155 and 0.12, respectively).

B. Optical-phonon spectra

One could, in principle, obtain the vibrational eigenmodes from the diagonalization of the dynamical matrix (once the relaxation procedure described above has been performed). In polar materials, both short-range interaction (covalent bonding) and long-range Coulomb interaction have to be taken into account. Such calculations have been performed recently for free-standing GaP dots with up to 2000 atoms.[23] In our case, this procedure is, however, impractical: our system, which includes necessarily a dot and a large part of the matrix, contains too many atoms (with regard to the simulation capabilities).

Moreover, the dot vibrational eigenmodes are collective excitations, involving all the atoms belonging to the dot. As an approximation, we shall therefore consider that the phonons experience the average strain field inside the dots. Owing to the rather homogeneous strain field inside the dots (Figs. 2 and 3), this should provide us with reasonable results. The frequencies of the optical phonon in presence of strain can be derived from the secular equation given in Ref. 24. The frequency shifts depend on the strain tensor ε_{ij} and the phonon deformation potentials $\tilde{K}_{ij}$. According to our modeling, the average shear strain components can be disregarded. As $\varepsilon_{xx}=\varepsilon_{yy}$, the strain splits the optical phonons into a singlet and a doublet component.[24,25] Their relative frequency shifts are given by

$$\left(\frac{\Delta\omega}{\omega_0}\right)_S = \frac{1}{2}\tilde{K}_{12}(\varepsilon_{xx}+\varepsilon_{yy}) + \frac{1}{2}\tilde{K}_{11}\varepsilon_{zz}, \tag{3}$$

$$\left(\frac{\Delta\omega}{\omega_0}\right)_D = \frac{1}{2}\tilde{K}_{11}\varepsilon_{xx} + \frac{1}{2}\tilde{K}_{12}(\varepsilon_{yy}+\varepsilon_{zz}). \tag{4}$$

The vibrations are along [001] for the singlet mode and in the plane normal to [001] for the doublet modes.[25] Notice that, depending on whether the longitudinal optical (LO) or transverse optical (TO) deformation potentials are used, the resolution of the secular equation provides us either with the LO singlet and the LO doublet or with the TO singlet and the TO doublet. Concerning Fig. 6 in Ref. 2, let us indicate that the peaks assigned to LO and TO correspond in fact to the histogram of the LO singlet and the LO doublet relative changes in phonon energy. One can easily identify three peaks for the dot: two having a similar location around 7% (i.e., the doublet) and another one around 10% (i.e., the singlet).

TABLE II. Strain (S=singlet) and confinement (conf) induced LO frequency shifts (in cm^{-1}) for *A* and *B* dot shapes. ''2D'' stands for a pseudomorphic 2 ML InAs layer in InP. ''exp'' denotes experimental data.

Shape	$\Delta\omega_S$	$\Delta\omega_{\mathrm{conf}}$	$\Delta\omega_{S+\mathrm{conf}}$	$\Delta\omega_{\mathrm{exp}}$
2D	12	−4	8	9
A	11.7	−0.2	11.5	12.1
B	11.3	≈0	11.3	11.8

According to Aoki *et al.*,[27] $(\tilde{K}_{11}+2\tilde{K}_{12})^{\mathrm{InAs}}_{\mathrm{LO}} = -6.4$ and $(\tilde{K}_{11}+2\tilde{K}_{12})^{\mathrm{InAs}}_{\mathrm{TO}} = -7.3$. According to Yang *et al.*,[28] $(\tilde{K}_{11}-\tilde{K}_{12})^{\mathrm{InAs}}_{\mathrm{TO}} = 0.51$. Unfortunately, $(\tilde{K}_{11}-\tilde{K}_{12})^{\mathrm{InAs}}_{\mathrm{LO}}$ has not been measured. The corresponding TO value has been used in most of the previous calculations. One has, however, to note that in III-V compounds, $(\tilde{K}_{11}-\tilde{K}_{12})_{\mathrm{LO}}$ is usually larger than $(\tilde{K}_{11}-\tilde{K}_{12})_{\mathrm{TO}}$.[26] On the other hand, Tran *et al.* did investigate strained InAs/InP superlattices combining Raman scattering and x-ray diffraction.[29] Their data can therefore be used to estimate $(\tilde{K}_{11}-\tilde{K}_{12})^{\mathrm{InAs}}_{\mathrm{LO}}$. One obtains $(\tilde{K}_{11}-\tilde{K}_{12})^{\mathrm{InAs}}_{\mathrm{LO}} = 0.92$, which is about twice as large as the corresponding TO value [thus, one observes the same trend as for GaAs and InP (Ref. 26)]. One finally obtains $\tilde{K}_{11} = -1.50$ and $\tilde{K}_{12} = -2.43$ for the InAs LO and $\tilde{K}_{11} = -2.09$ and $\tilde{K}_{12} = -2.60$ for the InAs TO.[30] According to measurements performed at room temperature on InAs (111), ω_0 equals 239.8 cm^{-1} and 218.8 cm^{-1} for the InAs LO and TO, respectively.

In backscattering geometry from the (001) surface, only the LO singlet is Raman-active. The calculated strain-induced frequency shifts of the LO singlet are reported in Table II. The shift expected for a pseudomorphic 2D layer is also given. Although the strain relaxation in these systems is quite different, the calculated strain-induced frequency shifts [Eq. (3)] are rather similar.

The island heights are small and confinement may modify the phonon frequencies. As the island widths are much larger, the effects of lateral confinement on the phonon frequencies can be neglected. From the island heights and the optical-phonon dispersion relation[29] (i.e., applying the usual linear chain model[25]), we have calculated the confinement induced frequency shifts $\Delta\omega_{\mathrm{conf}}$. The values of $\Delta\omega_{\mathrm{conf}}$ deduced in this way for the first-order confined mode are reported in Table II; $\Delta\omega_{\mathrm{conf}}$ is found to be very small for the 3 and 7 nm high islands. In our case, the frequency changes related to dot size fluctuations are thus also small.

III. COMPARISON WITH EXPERIMENT AND DISCUSSION

We present Raman spectra of a 2 ML InAs single quantum well sample (SQW) and a sample with *A*-type dots. De-

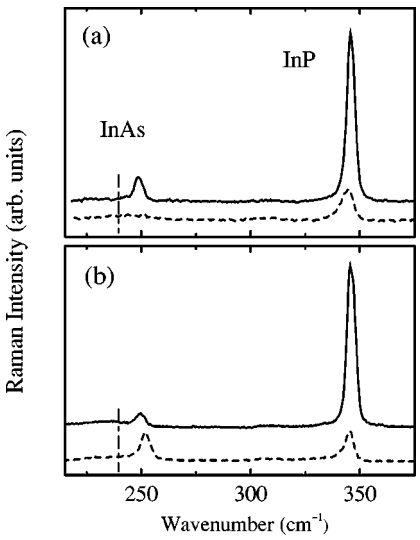

FIG. 4. Raman spectra: (a) 2 ML InAs/InP SQW, (b) type *A* dots, corresponding to 2.5 ML InAs deposited on InP and capped by 25 nm InP. Spectra were recorded with the $z(X,Y)\bar{z}$ crossed-polarization configuration (solid line) and with the $z(X,X)\bar{z}$ parallel-polarization configuration (dashed line), with $X=[100]$ and $Y=[010]$. The dot-dashed line indicates the bulk InAs LO frequency.

tails about the sample growth can be found in Refs. 10 and 21. The spectra were recorded at room temperature with an *XY* Dilor spectrometer equipped with a cooled charge coupled device detector. Depending on the excitation energy used (incoming or outgoing resonance), the Raman spectra display InAs confined phonon or/and interface (IF) mode peaks. As we intend to discuss the effects of strain on confined optical phonons, we only reported here (Fig. 4) spectra displaying confined LO-related peaks [scattering by TO phonons is forbidden in backscattering geometry from (001) surfaces]. The krypton laser lines we used are in incoming resonance with either the SQW or the dot InAs E_1-like transition [520.8 nm and 482.5 nm for Figs. 4(a) and 4(b), respectively].[10] We have been able to discriminate between the island-related signal and the WL-related one using different polarization configurations and the 2 ML SQW sample as a reference.[10] The InAs LO peaks related to the WL and the islands are observed in the crossed-polarization and parallel-polarization configurations, respectively. The InP substrate LO peak is observed in the crossed-polarization configuration. The peak observed in the parallel-polarization configuration in the InP frequency range is attributed to a symmetric InP-like interface mode (IF).[10,29] Despite the dot size fluctuations and the inhomogeneous strain fields, one observes rather sharp Raman lines (Fig. 4). This is likely due to (i) the weak dependence on the dot size of both $\Delta\omega_S$ and $\Delta\omega_{\text{conf}}$ and (ii) the fact that the phonons are collective vibrational modes (the inhomogeneous strain field inside the dot therefore does not induce significant line broadening).

The LO frequency shifts are reported in Table II. It is noteworthy that the WL and the 2 ML SQW LO frequencies are similar (Fig. 4). The calculations $\Delta\omega_{S+\text{conf}}=\Delta\omega_S+\Delta\omega_{\text{conf}}$ account rather well for the experimental data. Moreover, using grazing incidence, we were able to observe the InAs TO doublet peak (for dots with shape *A*). Its frequency is shifted up by $+7.2$ cm^{-1} with respect to the bulk InAs TO frequency. From the average strain components (for shape *A*) and the TO deformation potentials, we obtain [Eq. (4)] $\Delta\omega=6.8$ cm^{-1}, which is in good agreement with experiment (due to the very weak TO dispersion, confinement effects are negligible).

Notice that we did not take into account in our simulations that the dots are sometimes slightly elongated (one expects a little less strain relaxation and higher phonon frequencies). However, the main actual limitation we are concerned with (for either the comparison between the calculations and the experimental results or the experimental determination of the average strain values) is due to our poor knowledge of the phonon deformation potentials. The latter are indeed difficult to measure accurately.

It is noteworthy that if one is able to measure both the dot LO and TO frequencies, one can deduce the ε_{xx} and ε_{zz} average values by considering simultaneously Eqs. (3) and (4) (without any numerical strain simulation). Considering the experimental LO and TO frequency shifts reported here for *A*-type dots (Table II), one obtains $\varepsilon_{xx}=-2.92\%$, $\varepsilon_{zz}=2.82\%$, and $\varepsilon_{zz}/\varepsilon_{xx}=-0.93$; these values are very close to the ones predicted by the simulation (Table I). The relative differences between the experimental and calculated values do not exceed 4%. This good agreement supports the assumptions we made (in particular the one concerning the phonons probing the average strain field). Combining LO and TO Raman scattering provides thus a means of measuring average strain values in self-assembled dots.

The rather good agreement between the calculations and the experimental data suggests that the assumptions we made are reasonable. It also suggests that alloying inside the islands is not important. Optical phonons in InAsP alloys display the usual two-mode behavior: the InAs-like (InP-like) LO frequencies decrease with decreasing In (P) content.[31] If one considers InAsP dots (instead of InAs dots) in InP, the calculations yield lower phonon frequencies (due to the alloying induced frequency shift and the lower mismatch with respect to InP) which obviously do not account for the experimental data (Table II). Moreover, it has been shown that the formation of an intermediate InAsP alloy layer during the growth of InAs/InP structures gives rise to additional interface modes.[32] We do not observe the corresponding features in the Raman spectra.

One may wonder whether one can find some evidence in the Raman spectra for the strain inside the InP barriers. As most of the InP LO Raman signal originates from unstrained regions, we are not able to identify the contributions of the strained InP. The shift one expects from the tensile strain underneath the InAs dot (Fig. 2) and the InP LO deformation potentials[33] is very small (-0.5 cm^{-1}). On the other hand, one expects the InP-like IF to be sensitive to the strain around the islands.[14] However, as the IF frequencies depend also on both the island size and shape,[23,34,35] it is not obvious to obtain from the Raman spectra some reliable and quantitative information concerning the strained InP.

IV. CONCLUSION

In summary, we calculated the strain distribution in typical self-assembled InAs/InP (001) dots using the valence-

force-field method. The residual strain was shown to depend much on the dot shape. Even for rather flat dots, the average strain field is quite different from the 2D case. As the strain field penetrates deeply into the subtrate, a large part of the simulation cell has to be devoted to the subtrate.

We calculated the strain-induced frequency shifts, assuming the InAs phonons experience the average strain field inside the dot. It is shown that confinement does not modify much the dot phonon frequencies. Our calculations show good agreement with experimental results obtained by Raman scattering. Both the Raman spectra and the comparison between the calculated frequencies and the experimental values indicate that alloying effects are small.

Unlike electronic spectra, the dot phonon frequencies do not depend much on dot size. One can therefore analyze the dot phonon frequencies by (solely) considering the residual strain, and vice versa.

[1] S. Christiansen, M. Albrecht, H. P. Strunk, and H. J. Maier, Appl. Phys. Lett. **64**, 3617 (1994).

[2] M. Grundmann, O. Stier, and D. Bimberg, Phys. Rev. B **52**, 11 969 (1995).

[3] T. Benabbas, P. Francois, Y. Androussi, and A. Lefebvre, J. Appl. Phys. **80**, 2763 (1996).

[4] Y. Androussi, P. François, A. Lefebvre, C. Priester, I. Lefebvre, G. Allan, M. Lannoo, J. M. Moison, N. Lebouche, and F. Barthe, in *Evolution of Thin-Film and Surface Structure and Morphology*, edited by B. G. Demczyk, E. D. Williams, E. Garfunkel, B. M. Clemens, and J. E. Cuomo, Materials Research Society, Symposia Proceedings No. 355 (MRS, Pittsburgh, 1995), p. 569; C. Priester, I. Lefebvre, G. Allan, and M. Lannoo, in *Mechanisms of Thin Film Evolution*, edited by S. M. Yalisove, C. V. Thompson, and D. J. Eaglesham, Materials Research Society Symposia Proceedings No. 317 (MRS, Pittsburgh, 1994), p. 131.

[5] H. Jiang and J. Singh, Phys. Rev. B **56**, 4696 (1997).

[6] J. Kim, L.-W. Wang, and A. Zunger, Phys. Rev. B **57**, R9408 (1998), and references therein.

[7] R. Heitz, M. Grundmann, N. N. Ledentsov, L. Eckey, M. Veit, D. Bimberg, V. M. Ustinov, A. Yu Egorov, A. E. Zhukov, P. S. Kop'ev, and Zh. I. Alferov, Appl. Phys. Lett. **68**, 361 (1996).

[8] S. Fafard, R. Leon, D. Leonard, J. L. Merz, and P. M. Petroff, Phys. Rev. B **52**, 5752 (1995).

[9] B. R. Bennet, B. V. Shanabrook, and R. Magno, Appl. Phys. Lett. **68**, 958 (1996).

[10] J. Groenen, A. Mlayah, R. Carles, A. Ponchet, A. Le Corre, and S. Salaün, Appl. Phys. Lett. **69**, 943 (1996).

[11] G. Armelles, T. Utzmeier, P. A. Postigo, J. C. Ferrer, P. Peiró, and A. Cornet, J. Appl. Phys. **81**, 6339 (1997).

[12] P. D. Persans, P. W. Deelman, K. L. Stokes, L. J. Schowalter, A. Byrne, and T. Thundat, Appl. Phys. Lett. **70**, 472 (1997).

[13] J. Groenen, R. Carles, S. Christiansen, M. Albrecht, W. Dorsch, H. P. Strunk, H. Wawra, and G. Wagner, Appl. Phys. Lett. **71**, 3856 (1997).

[14] Y. A. Pusep, G. Zanelatto, S. W. da Silva, J. C. Galzerani, P. P. Galzerani, P. P. Gonzalez-Borrero, A. I. Toropov, and P. Basmaji, Phys. Rev. B **58**, 1770 (1998).

[15] S. H. Kwok, P. Y. Yu, C. H. Tung, Y. H. Zhang, M. F. Li, C. S. Peng, and J. M. Zhou, Phys. Rev. B **59**, 4980 (1999).

[16] A. A. Sirenko, M. K. Zundel, T. Ruf, K. Eberl, and M. Cardona, Phys. Rev. B **59**, 4980 (1999).

[17] M. J. P. Musgrave and J. A. Pople, Proc. R. Soc. London, Ser. A **268**, 464 (1962).

[18] P. N. Keating, Phys. Rev. **145**, 637 (1966).

[19] R. M. Martin, Phys. Rev. B **1**, 4005 (1970).

[20] J. L. Martins and A. Zunger, Phys. Rev. B **30**, 6217 (1984).

[21] A. Ponchet, A. Le Corre, H. L'Haridon, B. Lambert, and S. Salaün, Appl. Phys. Lett. **67**, 1850 (1995).

[22] See, for instance, Q. Xie, A. Madhukar, P. Chen, and N. Kobayashi, Phys. Rev. Lett. **75**, 2542 (1995).

[23] H. Fu, V. Ozoliņs, and A. Zunger, Phys. Rev. B **59**, 2881 (1999).

[24] F. Cerdeira, C. J. Buchenauer, F. H. Pollak, and M. Cardona, Phys. Rev. B **5**, 580 (1972).

[25] B. Jusserand and M. Cardona, in *Light Scattering in Solids V*, Topics in Applied Physics Vol. 66, edited by M. Cardona and G. Güntherodt (Springer, New York, 1989).

[26] See Table 3.1 in Ref. 25; $(\tilde{K}_{11}-\tilde{K}_{12})_{\mathrm{LO}}/(\tilde{K}_{11}-\tilde{K}_{12})_{\mathrm{TO}}$ equals 2.3 and 1.7 for GaAs and InP, respectively.

[27] K. Aoki, E. Anastassakis, and M. Cardona, Phys. Rev. B **30**, 681 (1984).

[28] M. J. Yang, R. J. Wagner, B. V. Shanabrook, W. J. Moore, J. R. Waterman, C. H. Yang, and M. Fatemi, Appl. Phys. Lett. **63**, 3434 (1993).

[29] C. A. Tran, J. L. Bredner, R. Leonelli M. Jouanne, and R. A. Masut, Phys. Rev. B **49**, 11 268 (1994); Superlattices Microstruct. **15**, 391 (1994).

[30] Notice that if one calculates the strain-induced LO frequency shifts using the $(\tilde{K}_{ij})_{\mathrm{LO}}$ derived from $(\tilde{K}_{11}+2\tilde{K}_{12})_{\mathrm{LO}}$ and $(\tilde{K}_{11}-\tilde{K}_{12})_{\mathrm{TO}}$ [instead of the $(\tilde{K}_{11}-\tilde{K}_{12})_{\mathrm{LO}}$ value we deduced from Ref. 29], one would obtain shifts which are typically 25% lower than those reported here (Table II).

[31] R. Carles, N. Saint-Cricq, J. B. Renucci, and R. J. Nicholas, J. Phys. C **13**, 899 (1980).

[32] L. G. Quagliano, B. Jusserand, and D. Orani, Phys. Rev. B **56**, 4919 (1997).

[33] E. Anastassakis, Y. S. Raptis, M. Hunermann, W. Richter, and M. Cardona, Phys. Rev. B **38**, 7702 (1988).

[34] P. A. Knipp and T. L. Reinecke, Phys. Rev. B **46**, 10 310 (1992).

[35] M. P. Chamberlain, C. Trallero-Giner, and M. Cardona, Phys. Rev. B **51**, 1680 (1995).